Title: Dynamic Reservoir Modeling for Water Security under Climatic and Anthropogenic Pressures in Aburrá Valley

Authors: Nathalia Jastrombek Vieira, Néstor Jaime Aguirre Ramírez and Fabio de Jesús Vélez Macías

Revista Facultad de Ingeniería, June 5, 2026

Dynamic Reservoir Modeling for Water Security under Climatic and Anthropogenic Pressures in Aburrá Valley

Modelación Dinámica de Embalses para la Seguridad Hídrica bajo Presiones Climáticas y Antropogénicas en el Valle de Aburrá

Authors: Double-blind review

KEYWORDS:
Reservoir modeling, Land use change, Climate change, Water security.

Modelación de embalse, Cambio de uso del suelo, Cambio climático, Seguridad hídrica.

ABSTRACT: Water security in Aburrá Valley, Colombia, relies heavily on the Riogrande II and La Fe reservoirs, which face increasing pressures from climate variability, land use change, and rising demand. Although SWAT+ is a powerful hydrological modeling tool, its reservoir module cannot represent dynamic changes in demand, land use, or external water inflow. To address these limitations, we developed resv_dyn, a Python algorithm that integrates: (i) annual land use changes derived from Dinamica EGO, (ii) progressive demand growth, and (iii) operation with pumped inflows from non-tributary rivers. The validation of resv_dyn was conducted using the Riogrande II Reservoir as a study case, comparing its performance with the SWAT+ reservoir module. The results show that resv_dyn effectively simulates the operational conditions of the reservoir, achieving outcomes comparable to those of SWAT+. Application to La Fe Reservoir under three climate scenarios shows that increased extreme rainfall temporarily boosts natural inflows, but these isolated peaks cannot be effectively stored due to reservoir capacity constraints. As a result, the system remains continuously dependent on pumping, and supply deficits are not substantially reduced. The proposed approach improves the representation of reservoir behaviour and provides a transferable tool for assessing reservoir resilience under combined climatic and anthropogenic pressures.

RESUMEN: La seguridad hídrica en el Valle de Aburrá, Colombia, depende en gran medida de los embalses Riogrande II y La Fe, los cuales enfrentan crecientes presiones asociadas a la variabilidad climática, el cambio de uso del suelo y el aumento de la demanda. Aunque SWAT+ es una herramienta poderosa para la modelación hidrológica, su módulo de embalses no permite representar cambios dinámicos en la demanda, el uso del suelo ni los aportes externos de agua. Para superar estas limitaciones, desarrollamos resv_dyn, un algoritmo en Python que integra: (i) cambios anuales de uso del suelo derivados de Dinamica EGO, (ii) crecimiento progresivo de la demanda y (iii) operación con aportes bombeados desde ríos no tributarios. La validación de resv_dyn se llevó a cabo utilizando el embalse Riogrande II como estudio de caso, comparando su desempeño con el módulo de embalses de SWAT+. Los resultados muestran que resv_dyn simula de manera efectiva las condiciones operativas del embalse, obteniendo resultados comparables a los de SWAT+.La aplicación al embalse La Fe bajo tres escenarios climáticos muestra que el aumento de lluvias extremas incrementa temporalmente los aportes naturales, pero estos picos aislados no pueden ser almacenados de manera efectiva debido a las limitaciones de capacidad del embalse. Como resultado, el sistema continúa dependiendo permanentemente del bombeo y los déficits de suministro no se reducen de forma sustancial. El enfoque propuesto mejora la representación del comportamiento de los embalses y ofrece una herramienta transferible para evaluar la resiliencia de los embalses frente a presiones combinadas de origen climático y antrópico.

1. Introduction

Urban water security refers to the ability to ensure sustainable and equitable access to safe water while protecting against water-related risks such as scarcity and pollution [1]. In Colombia's Aburrá Valley, the Riogrande II and La Fe reservoirs supply nearly 90% of domestic water consumption [2], making their long-term performance critical for regional water security. However, both are increasingly exposed to pressures from urban expansion, agricultural conversion, climate variability, and population growth, which alter infiltration, runoff generation, and reservoir inflows [3], [4], [5], while simultaneously driving higher water demand [6], [7].

Hydrological models such as SWAT+ are widely used to assess the impacts of land use and climate change on streamflow and reservoir inflows [8], [9]. While

SWAT+ offers features such as decision tables and a water allocation module, it presents limitations for representing complex reservoir operations and dynamic socio-environmental drivers. These include: (i) the inability to simulate external water transfers not routed from upstream subbasins, (ii) daily release values that may exceed operational constraints despite monthly compliance, and (iii) the lack of direct support for spatially explicit, year-by-year land use changes. Such limitations hinder the realistic representation of combined land use dynamics, climate impacts, and evolving water demands in water balance assessments. While other studies have explored the individual impacts of population, climate or land use change on hydrological processes such as river flow and sediment yield within watersheds, fewer have combined effects on reservoir performance, particularly in terms of water supply reliability [10]. In this paper we present a customized reservoir algorithm (resv_dyn), designed to overcome these limitations. The algorithm uses a couple of reference SWAT+ simulations, but integrates spatially explicit, time-varying land use modeling based on Dinamica EGO [11], [12], [13], continuous population-driven demand growth derived from municipal census projections, and operational constraints on releases. Its performance is evaluated against SWAT+ with the available reservoir sub-routine using the Riogrande II Reservoir as a validation case, and its applicability is demonstrated for the more complex operational scenario of the La Fe Reservoir. We hypothesize that the resv_dyn algorithm can reproduce reservoir operational dynamics with accuracy comparable to the SWAT+ reservoir module, while offering greater flexibility to incorporate spatially explicit land use change, population-driven demand growth, and supplementary inflows.

2. Methods

2.1 Reservoir Module

SWAT+ can manage reservoirs via decision tables, but it cannot directly model time-varying water demand or land use. To address this, a Python-based routine (resv_dyn) was developed to simulate continuous changes in demand, land use, and more realistic releases, computing reservoir volumes daily using the water balance equation.

$$V_{n+1} = V_n + V_{inflow,n} + V_{pcp,n} - V_{evap,n} - V_{outflow,n} - V_{withdraw,n} \quad (1)$$

where V_n is the reservoir volume on the beginning of the n'th day and the remaining components correspond to sources and sinks of water during the n'th day. In equation (1) V_{inflow} is the daily basin inflow, V_{pcp} is the precipitation over the reservoir, V_{evap} is the daily evaporated volume from the reservoir, $V_{outflow}$ is the daily release if the level goes above some safety level and, finally, $V_{withdraw}$ is the volume used to satisfy the total demand, which includes the ecologic demand, energy production and human consumption. The relation 1 is then iterated from a known initial reservoir volume V_0 up to the desired number of projection days (N). The overview of the Reservoir Module is presented in Figure 1.

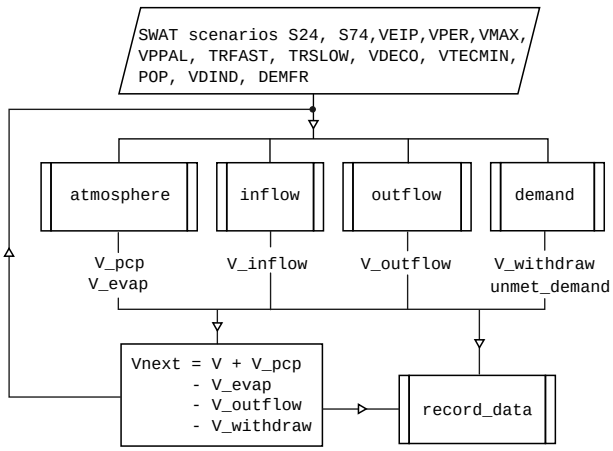

Figure 1 General overview of the resv_dyn module.

2.1.1 Water Inflow

The amount of water that arrives at the reservoir during the day can be calculated using SWAT+ for a given configuration of the land use, but it is difficult to consider temporal changes in the land management in the simulation, as it requires a new setup for each configuration or the use of decision tables that randomize the desired changes. Instead, we can calculate the inflow for every day in two fixed land-use scenarios obtained from a more sophisticated land use routine and the average n'th day water inflow as

$$V_{inflow,n} = \left(\frac{N-n}{N}\right) V_{inflow,n}(S24) + \left(\frac{n}{N}\right) V_{inflow,n}(S74) + V_{extra\_inflow,n}, \quad (2)$$

where N is the total number of days to be projected in the simulation. In general terms, equation 2 represents a weighted average between the inflows of two limiting scenarios, for instance S24 (land use 2024) and S74 (land use 2074), where the weights change in time linearly from 1 to 0 for S24 and from 0 to 1 for S74,

effectively transitioning smoothly from one scenario to the other, encoding the progressive changes in land use into the resulting reservoir inflow without requiring to perform sequential short simulations with slightly different land covers. The additional term V_{extra_inflow} accounts for additional artificial inflows like pumped water from a lower basin or channel. In the case of a pump system, the number of pumping units depends on the current level of the reservoir and availability of the lower source. A two-stage operation scenario was considered: (I) The reservoir volume is below VTECMIN and a strong pumping is used, and (II) the reservoir is below VPPAL and a slow pumping is used

$$V_{extra\_inflow}(I) = VPIN\_FAST, \quad (3)$$
$$V_{extra\_inflow}(II) = VPIN\_SLOW. \quad (4)$$

When reservoir levels fall below the technical minimum, natural inflows alone cannot meet demand, risking system failure. The pumping system is dimensioned to work alongside natural inflows, increasing the reservoir's capacity to meet the demand (Figure 2).

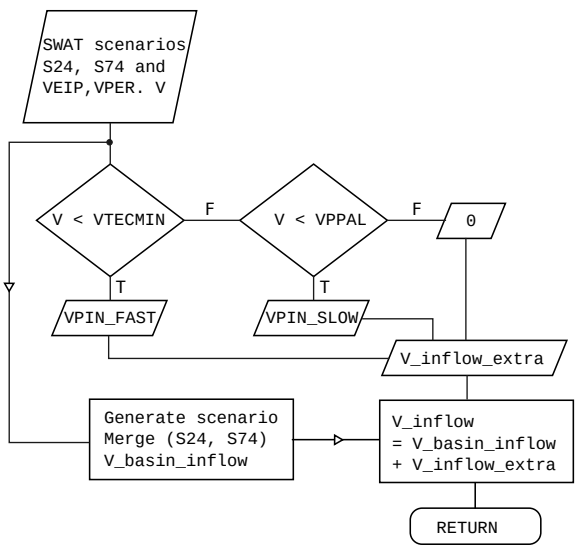

Figure 2 Overview of the Inflow subroutine, part of resv_dyn module.

2.1.2 Precipitation and Evaporation

Are obtained by multiplying the accumulated precipitation/evaporation during the day (m) by the current reservoir area (m^2). Since the total evaporated and precipitated volumes must be obtained from the climatic data, a simple reservoir simulation is performed with SWAT+. Since the reservoir module only returns total volumes (m^3), the accumulated values (in m) are obtained by dividing the total volumes by the total simulation reservoir area, then the resulting values are used to calculate the precipitation/evaporation total volume for the corresponding area in resv_dyn on each simulation day.

2.1.3 Outflow

For the water releases or outflow calculation three scenarios are considered: (I) The reservoir volume (Vres) is below the principal volume, (II) Vres is above the principal volume and below 95% of the maximum volume and (III) Vres is above 95% of the maximum volume. In scenario (I) there is no outflow, as the reservoir volume must increase to achieve its principal value (VPPAL). In the scenarios (II) and (III) the outflow is calculated by setting a corresponding recovery time (in days) for the reservoir to reach the principal value

$$V_{outflow}(II) = \frac{V_n - VPPAL}{TRSLOW}, \quad (5)$$
$$V_{outflow}(III) = \frac{V_n - VPPAL}{TRFAST}, \quad (6)$$

where $TRSLOW$ was set to 2 days of recovery and $TRFAST$ to 1 day. Notice that in scenario (III) the time is shorter to prevent reservoir overflow in the case of strong precipitations as the volume is close to the reservoir maximum. Since the other components of the water balance are not included in this calculation it is not expected that the system will return to the principal volume in the defined number of days, it can take more or less time depending on the current watershed inflow and precipitation. Figure 3 shows an overview of the algorithm of Outflow from the Reservoir Module.

2.1.4 Withdrawal

The withdrawal calculation is a little more involved, as it must take into account the water demand and the reservoir status. There are three scenarios of interest: (I) The reservoir is above the technical minimum (VTECMIN), (II) The reservoir is below the technical minimum and above the permanent volume (VPER), and (III) The reservoir is below the permanent volume. The base demand from the reservoir has the form

$$base\_demand = VDECO + DEMFR \times POP \times VDIND + EXTRA\_OUT, \quad (7)$$

where $VDECO$ is the daily ecological volume, $DEMFR$ is the fraction of the city demand satisfied by the reservoir, POP is the total population and

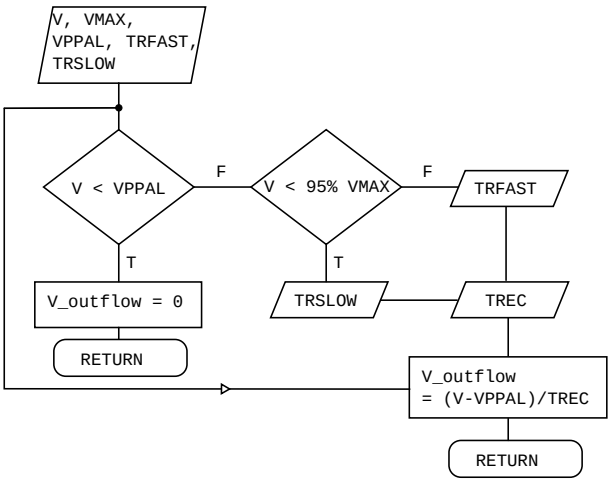

Figure 3 Overview of the Outflow subroutine, part of resv_dyn module.

$VDIND$ is the individual daily demand. The extra outflow $EXTRA\_OUT$ includes known demands for other uses or unspecified populations connected to the reservoir. There are tabulated values for the individual daily demand that take into account human needs and network losses, however they do not consider other uses that take place from economic activities or city maintenance. These activities are nonetheless related to the current population levels, as more population directly affects the level of economic and maintenance activities. To determine a realistic value of $VDIND$, reference values obtained from the operation of the potabilization plant are used with the known value of $DEMFR$. For instance, consider that the population and operation of the plant are known at some point in time (POP_REF, $DEMAND\_REF$), then, $VDIND$ can be obtained from the previous equation at that moment in time

$$VDIND = \frac{OPER\_REF}{POP\_REF \times DEMFR}. \tag{8}$$

Depending on the reservoir level there are two different levels of energy production so as to prioritize human consumption over energy production.

$$demand(I) = base\_demand + reg\_erg\_demand\_day, \tag{9}$$

$$demand(II) = base\_demand + min\_erg\_demand\_day, \tag{10}$$

$$demand(III) = base\_demand + min\_erg\_demand\_day, \tag{11}$$

where $reg\_erg\_demand\_day$ is the volume of water to satisfy the regular energy demand and $min\_erg\_demand\_day$ is some volume of water to satisfy a lower energy demand when the energy production can compromise the water treatment. When the reservoir falls below the permanent level the withdrawal can not occur, in that case the required volume becomes an unmet demand

$$V_{widthdraw}(I) = demand(I), \tag{12}$$

$$V_{widthdraw}(II) = demand(II), \tag{13}$$

$$V_{widthdraw}(III) = 0, \tag{14}$$

$$V_{unmet} = demand(III), \tag{15}$$

Although the evolution is calculated daily, the results are later added to express them on a monthly basis that is more useful in an engineering setting. Figure 4 presents the Demand subroutine logic.

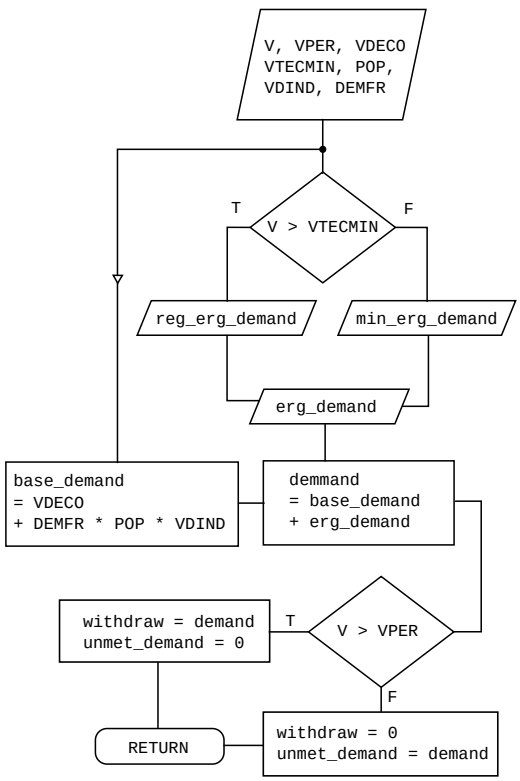

Figure 4 Overview of the Demand subroutine, part of resv_dyn module.

The implementation in Python 3.12 of the Reservoir Dynamics module (resv_dyn) is provided in Appendices.

2.2 Application: Riogrande II and La Fe reservoirs

2.2.1 Study area description

The Aburrá Valley is located in the Central Cordillera in the northern part of the Colombian Andes, covering

an area of 1,152 km². The valley has a population of approximately 3.5 million inhabitants, concentrating 59% of the department population in just 1.8% of Antioquia's area [14], [15]. The Aburrá Valley exhibits a humid tropical climate, characterized by a bimodal precipitation regime with rainfall peaks typically occurring between April–May and October–November. Average annual precipitation ranges from 1400 to 2700 mm, and average temperature of 22ºC [16]. The water supply for the region is mostly provided by the Riogrande II and La Fe reservoirs. Both reservoirs have multiple uses, including hydroelectric power generation, potable water supply, and recreation.

The Riogrande II Reservoir has a capacity of 185 million cubic meters [17], covering an area of 1,169 hectares. Its main tributaries are the Grande River, the Chico River, and the Las Ánimas stream [18]. The catchment area of the Riogrande II reservoir is located in mountainous terrain, with elevation varying between 2,220 and 3,346 meters above sea level. In 2020, land use in this watershed is dominated by Mosaic of Agriculture and Pasture (63%), followed by Forest (28%) [19]. Soils are primarily composed of Ultisols, followed by Inceptisols [20]. A reservoir diversion supplies water to the Manantiales Water Treatment Plant (WTP Manatiales) that has a design flow of 6 m^3/s, with plans to expand to 9 m^3/s; it currently operates at 4.3 m^3/s, supplying approximately 40% of the population of the Aburrá Valley [21], [2], [22].

The La Fe Reservoir has a capacity of 12 million cubic meters, covering an area of 1.33 km². The elevation of La Fe reservoir watershed varies from 2,121 and 2,925 meters above sea level [18]. The most present soil type is the Ultisols [20] and the land use in this watershed in 2020 was mostly Forest (55%), followed by Mosaic of Agriculture and Pasture (37%) [19]. The La Ayurá Water Treatment Plant (WTP La Ayurá), that is feeded by the Le Fe Reservoir, has a capacity of 9.2 m^3/s but is currently operating with a flow of 4.6 m^3/s [22], serving 50% of the population of Aburrá Valley [2].

Its natural tributaries are the Espíritu Santo, Las Palmas, San Luis, Boquerón, Potreros, and La Miel streams, and it also receives water through pumping from the Buey ($2m^3/s$), Piedras ($2m^3/s$) and Pantanillo ($3.10m^3/s$) rivers, the latter contributing 6 m^3/s during dry seasons. The system operates since the end of 2005, with a maximum of four pump units operate simultaneously, with 1.5 m^3/s each [18], [22], [23], [24]. Both Riogrande II and La Fe reservoir watersheds are presented in Figure 5.

2.2.2 Population projection

For the population projection, urban census data from the National Administrative Department of Statistics (DANE) between 1938 and 2018 (eight censuses) were used [25], [26], [27], [28], [29], [30], [31], [32] (Appendices, Table 4). A Logistic Growth Model was applied, as annual municipal growth rates generally declined over time (Appendices, Figure 18). Due to the limited number of observations, DANE's municipal projections for 2020–2035 [33] were incorporated, totaling 24 years of data. Figure 6 shows projections for each municipality in the Aburrá Valley and for the region as a whole. The model fit both census data and official projections well ($R^2 \geq 0.97$ for all municipalities).

According to Figure 6, Medellín city remains the most populous, reaching 2,931,774 inhabitants (65.5% of the total) by 2074, followed by Bello with 659,387 (14.3%). Envigado and Sabaneta surpassed Itagüí around 2005 and together grew by 24.52% over the projection period. Barbosa and La Estrella show the highest growth rates (37.78% and 32.77%), while Itagüí (13.72%), Medellín (14.40%), and Copacabana (15.78%) have the lowest. By 2074, the valley's population is projected at 4,620,033, a 16.88% increase from the 2024 estimate of 3,992,029 inhabitants[33]. These results suggest that the Aburrá Valley is nearing population saturation.

2.2.3 Land use change projection

The projection of land use changes in the Riogrande II and La Fe reservoirs watersheds was modeled using the Dinamica EGO (Environment for Geoprocessing Objects) software. This free, user-friendly platform allows the construction of spatially explicit environmental models, ranging from simple to highly complex. It integrates standard GIS functions with specialized land change simulation tools, such as cellular automata and calibration algorithms [11], [12], [13]. To model the land use and land cover change of theRiogrande II and La Fe reservoir watersheds it was used the land use change algorithm as described in the software documentation, MODULE VIII [34].

The calibration and validation of the model was conducted using the MapBiomas Colombia Collection 1 data [19]. It provides annual LULC maps from 1985 to 2022 at 30-meter resolution. These maps were created using pixel-by-pixel Landsat classification and machine learning in Google Earth Engine [35]. Eight land use classes were present in at least one study area: Forest, Pinus, Other Non-Forest Formation, Mosaic of Agriculture and Pasture, Urbanization, Other Non-Vegetated Cover, Mining, and Water Bodies.

For this research, the period 2000–2020 was selected for model calibration and validation to reflect recent land change dynamics. The LULC models for both watershed showed to have a good performance for the Riogrande II watershed, while an acceptable

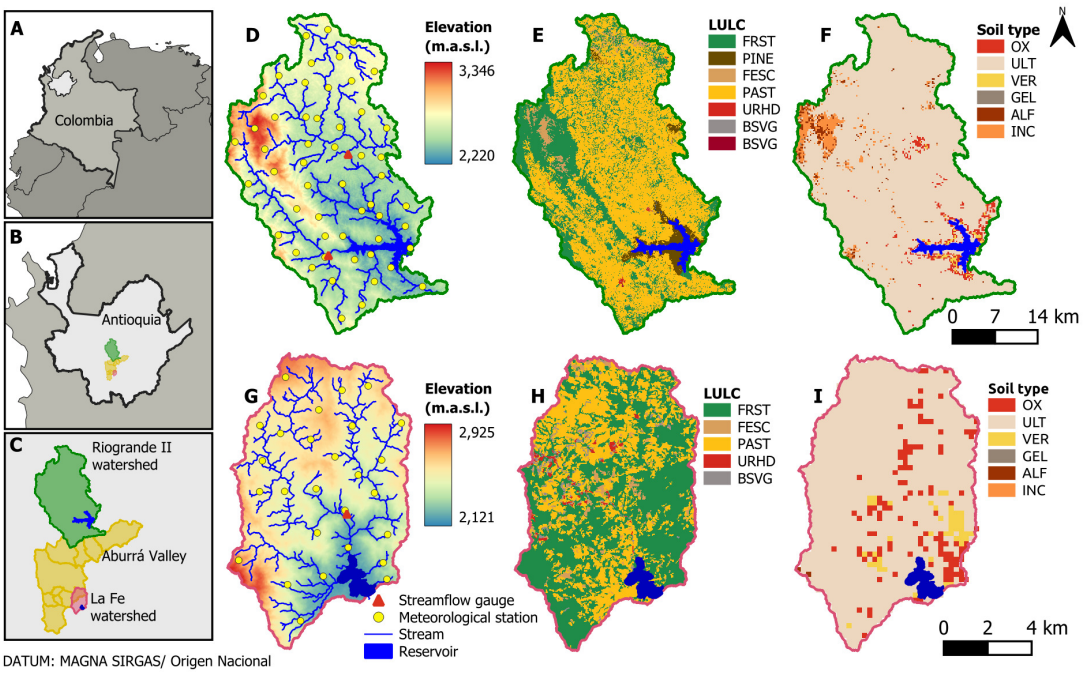

Figure 5 (A - C) Study area general location (Colombia, Antioquia, Aburrá Valley, respectively). (D, G) Riogrande II and La Fe reservoir watersheds elevation (m.a.sl.), respectively, including the meteorological and streamflow stations. (E, H) Riogrande II and La Fe reservoir watersheds land use and land cover, in the year 2020. (F, I) Riogrande II and La Fe reservoir watersheds soils type. The LULC and soils type codes are: FRST: Forest, PINE: Forest plantation, FESC: Other non-forest formation, PAST: Mosaic of agriculture and pasture, URHD: Urbanization, BSVG: Mining and Other non-vegetated area, OX: Oxisoils, ULT: Ultisoils, VER: Vertisoils, GEL: Gelisoils, ALF: Alfisoils, INC: Inceptisoils.

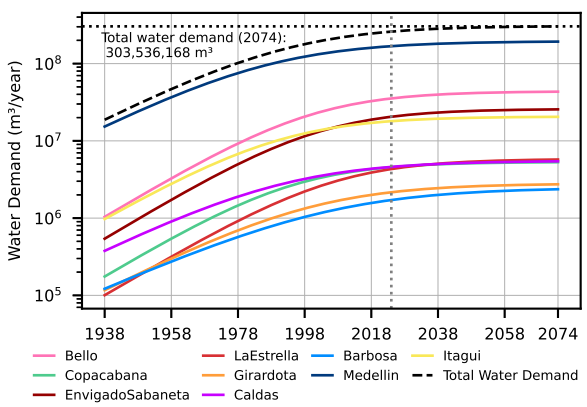

Figure 6 Demographic growth for the Aburrá Valley municipalities projected from 2024 to 2074. La Estrella municipality adjustment obtained a R^2 equal to 0.97. The other municipalities adjustments had a R^2 equal to 0.99.

performance for the La Fe watershed, based on the pixel-to-pixel metrics Figure of Merit, Producer's and User's Accuracy (Appendices, Table 5) and on the multiple window similarity analysis (Appendices, Figure 19).

Figure 7 presents the land use and cover projection for the period 2024 - 2074, for the Riogrande II and La Fe reservoirs watershed.

In the Riogrande II watershed (Figures 7A, 7B, 7C), the dominant land use is Agriculture and Pasture Mosaic, followed by Forest cover. Over the course of the projection period, Forest cover is expected to decrease from 33% to 18.5%, while the Agriculture and Pasture Mosaic is projected to expand, from 57% to 76% of the watershed area. The Other non-forest formation, that represents the Páramo ecosystem, is also anticipated to decline sharply, shrinking from 9% to just 1.35%. Although urban areas occupy a relatively small portion of the watershed, urbanization is projected to increase 12 times by 2074, reaching 0.36% of the total area.

In the La Fe watershed (Figures 7D, 7E, 7F), Forest remains the dominant land cover until around 2040, when it is overtaken by the Agriculture and Pasture Mosaic. Over the study period, Forest is projected to decline significantly, from 56.5% to 32.2%, while the Agriculture and Pasture Mosaic increases from 36.4% to 51.75%. Urbanization shows the most dramatic growth, expanding nearly 800 times, from virtually 0% to approximately 5% of the watershed area by the end of the projection period. Similarly,

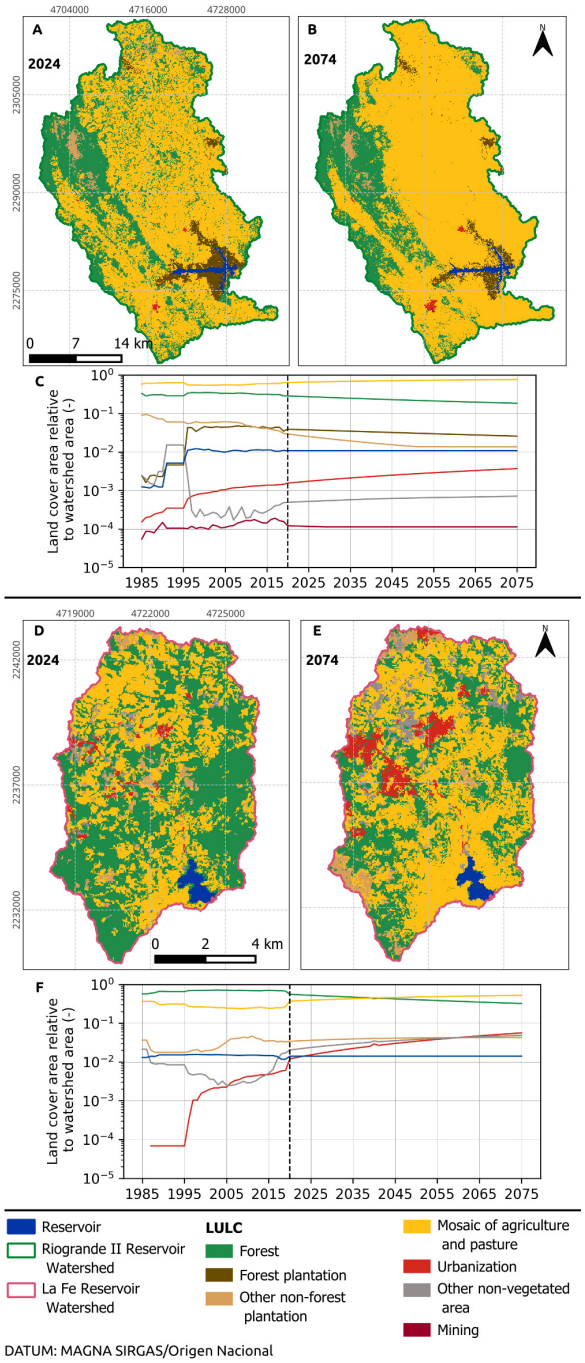

Figure 7 Land use change projections for the Riogrande II (A and B) and La Fe (D and E) watersheds for the period of 2024 - 2074. Land use area relative to the watershed area of Riogrande (C) and La Fe (F) watersheds.

Other Non-Vegetated Areas are expected to grow substantially, increasing about 20 times, from 2% to 5% of the total area.

The projected land use changes in both the Riogrande II and La Fe watersheds is consistent with the ongoing and increasing human pressure on natural ecosystems. Natural Forest and Páramo ecosystems are the most affected land covers, primarily due to the expansion of the Agriculture and Pasture Mosaic, which shows significant growth in both regions.

2.2.4 Climate change scenarios

The GFDL-CM4 model was selected for its ability to reasonably reproduce seasonal precipitation and near-surface air temperature patterns in Colombia [36], [37]. Daily maximum and minimum temperature, precipitation, and solar radiation at 1° × 1° resolution were obtained from the Earth System Grid Federation (ESGF) [38], extracted for nine grid cells covering the watersheds, and processed for bias correction.

Two CMIP6 climate change scenarios were used: SSP2-4.5, a stabilization pathway with GHG emissions peaking mid-century, leading to 4.5 W/m² radiative forcing in 2100, and SSP5-8.5, a high-emissions pathway with continued fossil-fuel development, minimal mitigation, leading to 8.5 W/m² by 2100 [39], [40]. These represent intermediate to extreme warming and are widely applied in CMIP6-endorsed Model Intercomparison Projects (MIPs). Both were compared to a Reference scenario cycling historical precipitation, temperature, and solar radiation records.

2.2.5 Bias correction

Statistical bias correction adjusts systematic deviations in climate model outputs using historical observations. A historical period (1994–2023) with overlapping observed and simulated data was used for training, assuming stationarity in the observation–model relationship [41]. The Quantile Delta Mapping (QDM) method [42] was applied, as it corrects the entire distribution while preserving climate change signals across quantiles, including the extremes. This is critical for hydrological applications sensitive to precipitation variability and temperature extremes.

Bias correction was implemented with the QuantileDeltaMapping function from the xclim Python library [43], adjusting each quantile using empirical CDFs of historical observations and model outputs. The resulting bias-corrected daily series of precipitation, maximum and minimum temperature, and solar radiation were used as inputs for hydrological simulations assessing reservoir system performance under projected climate scenarios.

2.2.6 SWAT+ hydrological modeling

In order to obtain the reservoir inflow, the precipitation that occurs over the reservoir and the evaporation from it, it was conducted a hydrological modeling using SWAT+ model. The input data for topography, soil type, land use and land cover, and climate were

obtained from various sources (Table 1). Slope classes were derived from a 12.5 m resolution Digital Elevation Model (DEM) and categorized into five ranges: 0–5%, 5–15%, 15–40%, 40–60%, and >60%.

Table 1 SWAT+ input data.

DATA	DESCRIPTION	SOURCE
Digital Elevation Model	Elevation data at a resolution of 12.5 m	ALOS PALSAR [44]
Soil type	Soil map of the La Fe watersheds, 250 m resolution	DSOLMap [20]
Land use & Land cover	Annual land use/cover (2000–2020), 30 m resolution	MapBiomas Colombia [19]
Precipitation	Daily gridded data, 0.05° resolution	CHIRPSv2 [45]
Temperature and solar radiation	Hourly gridded data, 0.25° resolution	ERA5 [46]

The soil map and parameters were derived from the Digital Soil Open Land Map (DSOLMap), a global 250 m dataset compatible with SWAT+ [20]. The original six-horizon profile was simplified to three horizons with a total depth of 2 m to reduce model complexity and improve groundwater representation.

Climate data were interpolated to create station-based time series. Virtual station density was set by watershed area: one per 20 km² for Riogrande II (53 stations) and one per 3 km² for La Fe (27 stations), distributed to capture topographic and land-use variability (Figure 5). Inputs included daily precipitation from CHIRPSv2 (0.05°) and hourly temperature and solar radiation from ERA5 (0.25°). CHIRPSv2 was selected for its performance in representing Colombian precipitation [47]. ERA5 hourly temperatures were aggregated to daily minimum and maximum, with a -6.5 °C/km lapse rate applied for elevation adjustment. ERA5 solar radiation was aggregated to daily values. Potential evapotranspiration (PET) was estimated with the Priestley–Taylor equation [48], and streamflow routing used the Muskingum method [49].

Calibration targeted parameters related to runoff generation, soil properties, and aquifer processes, following SWAT+ documentation. Monthly streamflow calibration employed the Dynamically Dimensioned Search (DDS) algorithm (500 iterations) [50] via SWAT+ Toolbox v3.0.6 . For Riogrande II, streamflow records from the Río Chico and Puente Belmira stations [51], [52] supported calibration for 1997–2008 and validation for 2009–2015. For La Fe, calibration for 1993–1995 and validation for 1996 relied on data from the Las Palmas station, the reservoir's main natural contributor [53]. Historical streamflow curves were digitized from the cited studies using automeris.io. Calibration and validation results were satisfactory for both watersheds. Calibrated parameters and performance metrics are provided in Table 6 and Figures 20, 21 and 22 on the Appendices section.

2.2.7 Reservoirs configuration

The Riogrande II and La Fe reservoir systems are interconnected through the supply network. Each reservoir supplies a different water treatment plant (WTP), but the treated water is distributed via an integrated urban supply system that serves the Aburrá Valley. Figure 8 illustrates the operational structure of the system.

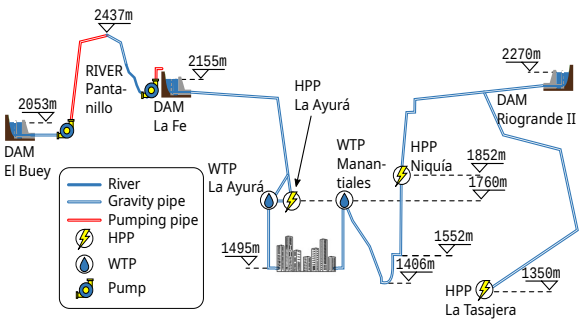

Figure 8 Diagram of the Riogrande II and La Fe reservoir systems.

As shown in Figure 8, water from the Riogrande II reservoir is withdrawn through two main outlets. One flow is directed to the La Tasajera hydropower plant (HPP) and then discharged into the Medellín-Aburrá River. Another withdrawal supplies the Niquía HPP and subsequently flows to the Manantiales WTP, which distributes treated water to the Aburrá Valley [22].

The Riogrande II reservoir relies entirely on natural inflows from its own watershed. In contrast, the La Fe reservoir depends on a more complex system involving inter-basin water transfers based on pumping infrastructure. Water is first diverted from the El Buey reservoir through a tunnel into the Piedras River. From there, it is pumped into the Pantanillo River, where up to 6 m³/s can be further pumped directly into the La Fe reservoir [22]. Water withdrawn from the La Fe reservoir passes through the La Ayurá HPP before reaching the La Ayurá WTP, which supplies treated water to the regional distribution network. Water uses for both reservoirs include energy generation, human consumption, and environmental flow, summarized in Table 2.

Table 2 presents two operational scenarios for the Riogrande II reservoir, differing in the water flow

Table 2 Summary of water uses and allocation thresholds for the Riogrande II and La Fe reservoirs, including withdrawals for energy generation, human consumption, and environmental flow [54], [55], [22]. *The non-environmental flow for La Fe Reservoir goes through the energy generation stage and later enters the treatment facility (so it only is counted once), while in the Riogrande II reservoir the flow is split for these usages.

RESERVOIR	USE	REG FLOW (m^3/s)	EXCEP FLOW (m^3/s)
Riogrande II	Energy generation	26.50	13.25
	Human consumption	4.30	4.30
	Environmental flow	13.27	13.27
	Total	44.07	30.82
La Fe	Energy generation	5.20	5.20
	Human consumption	5.20	5.20
	Environmental flow	4.35	4.35
	Total*	9.55	9.55

allocated for hydropower generation. Normal operation occurs when the reservoir water level is above the technical minimum volume, allowing greater water use for energy production. Exceptional operation occurs when the water level falls below the technical minimum, in which case only one turbine is operated for power generation.

The information required to configure volumes and areas of the Riogrande II and La Fe reservoirs is summarized in Table 3. These data were derived from bathymetric studies conducted by Empresas Públicas de Medellín [17],[56], [57]. Also, the water withdrawal from each reservoir was governed by operational rules reflecting storage-dependent management and are computed at the end of each daily time step. Since no information about the initial reservoir volumes at the simulation starting date was available , it was assumed that the reservoirs began at 80% of principal storage capacity.

Table 3 Summary of the configuration parameters for the Riogrande II (RGII) and La Fe reservoir

PARAM.	DESCRIPTION	RGII	LA FE
Principal vol. (Mm^3)	Volume of water needed to fill the reservoir to the principal spillway	185.26	11.33
Principal area (ha)	Reservoir surface area when reservoir is filled to principal spillway	980.00	126.00
Emergency vol. (Mm^3)	Volume of water needed to fill the reservoir to the principal spillway	235.99	13.53
Emergency area (ha)	Reservoir surface area when reservoir is filled to emergency spillway	1152.00	138.00
Initial vol. (Mm^3)	Reservoir volume at the beginning of simulation	148.21	9.06

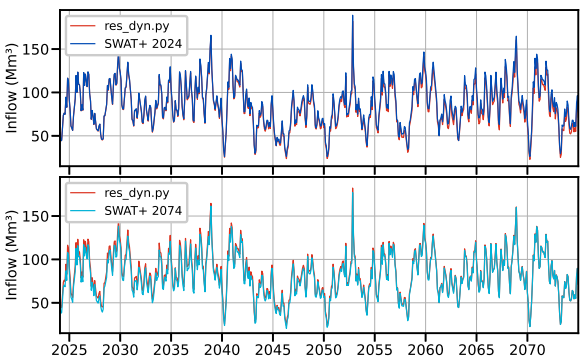

Figure 9 Monthly water inflow curves for the simulation using the land use map of 2024 (top), the land use map of 2074 (bottom) and the average curve between these two land use simulation scenarios.

3. Results

3.1 Validation: SWAT+ reservoir module vs. resv_dyn

The Riogrande II reservoir was used to validate the algorithm, since it does not have a pumped inflow and can be directly comparable to the results of the SWAT + reservoir module. Figure 9 shows the monthly water inflow to Riogrande II reservoir for simulations using the 2024 and 2074 land use maps, with the average inflow curve given by Equation 2.

It is possible to observe in Figure 9 that the average water inflow curve resulting from the resv_dyn algorithm smoothly transitions from the S24 scenario to the S74 scenario, without abrupt changes. As expected, at the beginning of the study period, the average curve resembles the 2024 land use scenario, and as we approach 2074, the average curve increasingly resembles the 2074 land use scenario.

From Figure 9 it is clear that the modeled changes in land use do not significantly alter the net water inflow to the reservoir but only slightly its time distribution. However, replacing natural covers by agriculture can

have significant effects on sediment transport, water quality, and reservoir algae blooming, which are not addressed in this work.

Figures 10 and 11 show the comparison of the SWAT+ reservoir module and the algorithm for daily and monthly water outflow and storage, respectively.

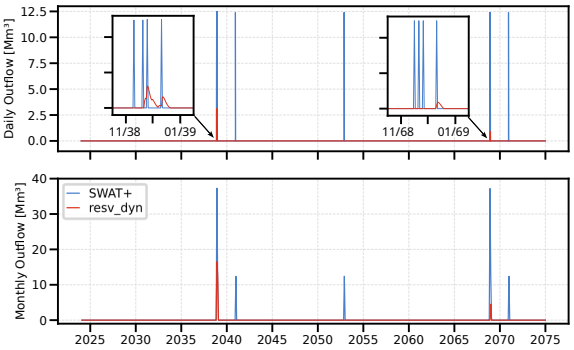

Figure 10 Comparison between the daily (top) and monthly sum (bottom) releases from the reservoir obtained from SWAT+ and the resv_dyn algorithm.

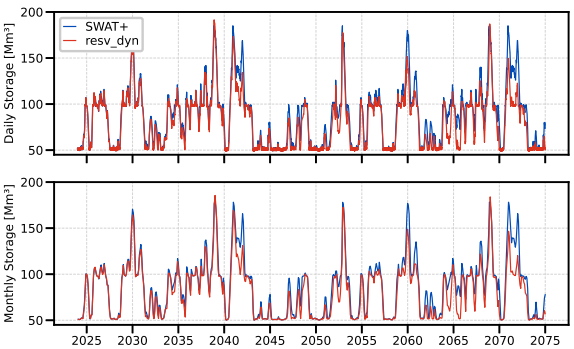

Figure 11 Comparison between the daily (top) and monthly average (bottom) storage of the reservoir obtained from SWAT+ and the resv_dyn algorithm.

In Figure 10, the SWAT+ curve exhibits more frequent and pronounced outflow events than resv_dyn. Another notable difference between the two reservoir modules is the magnitude of the outflows. In the daily graph, SWAT+ records peaks exceeding 12 Mm^3 or a daily average flow of 139 m^3/s, whereas the maximum outflow from resv_dyn is approximately 3 Mm^3 or a daily average flow of 34.7 m^3/s. The Grande river after the dam has an average flow of 35 m^3/s [51], suggesting that the SWAT+ prediction may substantially exceed typical downstream conditions and potentially alter the river's natural regime.

The reference SWAT+ simulation in Figures 10 and 11 fixed values for the population and land use (2024), so that the resv_dyn results are very similar at the beginning of the period. However, as time progresses the resv_dyn water demand grows, due to increases in population and economic activity, leading to a slow decrease in storage with respect to the fixed SWAT+ scenario.

Given that the resv_dyn algorithm successfully simulates the operational conditions of the Riogrande II Reservoir with results comparable to those produced by SWAT+, it can be assumed that the algorithm is more suitable for modeling the La Fe Reservoir, which operates under more complex conditions, including reduced capacity (respect to Riogrande II) and pumping from other sources.

3.2 Application: La Fe Reservoir dynamics under Climate Change

As mentioned in the study area description, to maintain the operational capacity of the La Fe reservoir, it is required to pump water from non-tributary rivers (Buey, Piedras and Pantanillo). This additional requirement can not be accommodated in SWAT+ but can be directly included in the resv_dyn routine and integrated in reservoir operation rules. Figures 12, 13 and 14 presents the graphs of monthly inflow, extra inflow, total inflow, outflow, and average storage volume for the Reference, Moderate, and Extreme climate scenarios, respectively, for the La Fe Reservoir, throughout the research period.

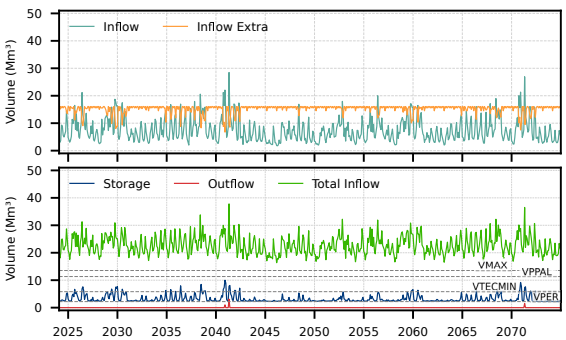

Figure 12 Monthly reservoir dynamics (2024-2074) for the Reference climate scenario for the La Fe Reservoir. The dashed gray horizontal lines indicate the operational water levels in the reservoir: VPER: Permanent volume; VTECMIN: Technical minimum volume; VPPAL: Principal volume; VMAX: Maximum volume.

As observed Figures 12, 13 and 14, additional pumping is permanently required in all scenarios but as climate scenarios intensify inflow peaks become more intense and frequent (due to stronger precipitation events), leading to an increase in natural inflow into La Fe reservoir in the climate change scenarios in relation to the Reference scenario. The average inflow of the Reference scenario is 7.51 Mm^3, with the peak

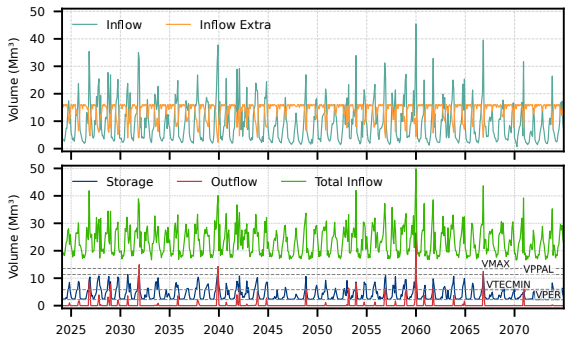

Figure 13 Monthly reservoir dynamics (2024-2074) for the Moderate climate scenario for the La Fe Reservoir. The dashed gray horizontal lines indicate the operational water levels in the reservoir: VPER: Permanent volume; VTECMIN: Technical minimum volume; VPPAL: Principal volume; VMAX: Maximum volume.

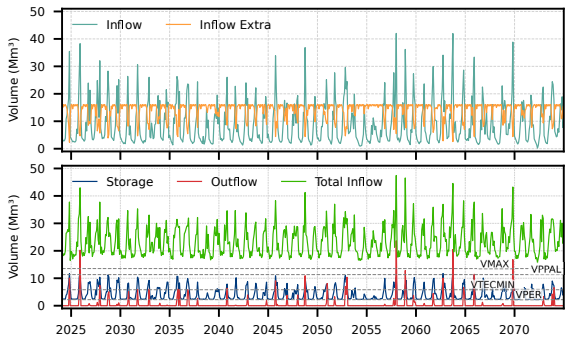

Figure 14 Monthly reservoir dynamics (2024-2074) for the Extreme climate scenario for the La Fe Reservoir. The dashed gray horizontal lines indicate the operational water levels in the reservoir: VPER: Permanent volume; VTECMIN: Technical minimum volume; VPPAL: Principal volume; VMAX: Maximum volume.

inflow reaching around 37 Mm³. In contrast, the Moderate and Extreme scenarios show higher average inflows of 9.34 Mm³ and 9.15 Mm³, respectively. In both scenarios, peak inflow events frequently exceed 20 Mm³, with one event reaching approximately 50 Mm³. As a consequence, dependency on pumped inflow ("extra inflow") decreases as climate change intensifies. The ratio of extra inflow to total inflow is 67% in the Reference scenario, compared to around 60% in both the Moderate and Extreme scenarios. Because of the limited capacity of the reservoir, the opposite trend is observed for water releases: the ratio of outflow to inflow is 0.12% in the Reference scenario, 4.17% in the Moderate scenario, and 5.82% In general, increases in natural inflow help to reduce the reliance on external sources, but the reservoir is unable to absorb the peak inflow events, resulting in water losses that could otherwise be used to meet demand.

Figures 15, 16, and 17 show the monthly average water storage, total demand, withdrawals, and unmet demand for the La Fe reservoir throughout the research period, for the Reference, Moderate and Extreme climate scenarios, respectively.

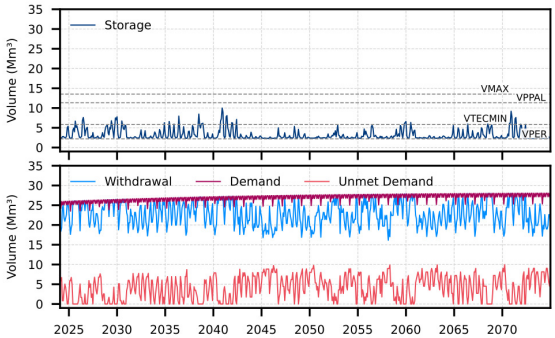

Figure 15 Monthly water demand for the Reference climate scenario for the La Fe Reservoir (2024-2074). The dashed gray horizontal lines indicate the operational water levels in the reservoir: VPER: Permanent volume; VTECMIN: Technical minimum volume; VPPAL: Principal volume; VMAX: Maximum volume.

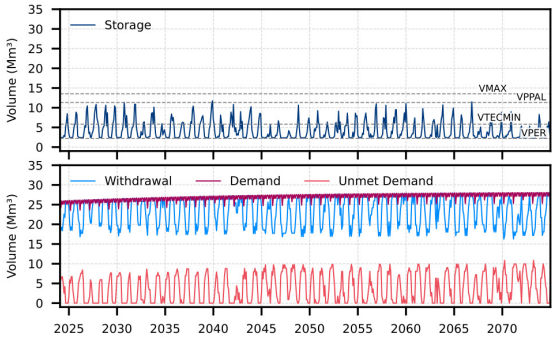

Figure 16 Monthly Water demand for the Moderate climate scenario for the La Fe Reservoir (2024-2074). The dashed gray horizontal lines indicate the operational water levels in the reservoir: VPER: Permanent volume; VTECMIN: Technical minimum volume; VPPAL: Principal volume; VMAX: Maximum volume.

From Figures 15, 16, and 17, the ratio of unmet demand / demand for the Reference scenario is 15.46%, 14.29% for the Moderate scenario and 15.49% for the Extreme scenario. It is interesting to note that, although there is a reduced reliance on pumping in all climate change scenarios, that does not translate to systematic reduction of the unmet demand because of the limited capacity of the reservoir.

The La Fe reservoir demonstrates a particularly high dependence on pumped inflows, which comprise at least 60% of its total inflow, at the same time exhibits relatively stable performance, but a high

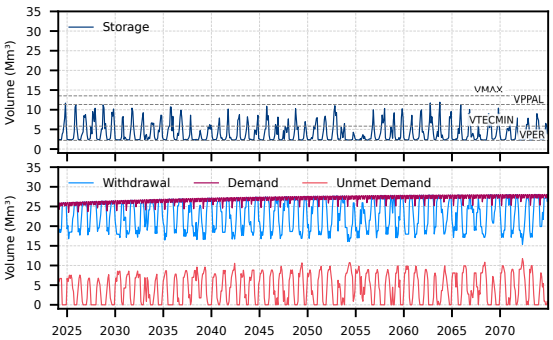

Figure 17 Monthly Water demand for the Extreme climate scenario for the La Fe Reservoir (2024-2074). The dashed gray horizontal lines indicate the operational water levels in the reservoir: VPER: Permanent volume; VTECMIN: Technical minimum volume; VPPAL: Principal volume; VMAX: Maximum volume.

unmet demand/demand ratio around 15%. While this research assumes the availability of an unlimited water supply from the Buey-Piedras-Pantanillo rivers system, this assumption may not hold under more severe climate or upstream usage conditions.

4. Discussion and Conclusions

This work presented resv_dyn, a customized reservoir simulation routine based on SWAT+ results, designed to overcome key limitations of its reservoir module in representing complex operational conditions. The method allows explicit integration of external water transfers, spatially explicit and time-varying land use changes through tools like Dinamica EGO, and population-driven demand growth, enabling more realistic simulations of reservoir behavior under combined climatic and anthropogenic pressures.

Applied to the La Fe Reservoir, the algorithm successfully replicated operational practices such as permanent pumping from non-tributary rivers and revealed how climate-driven inflow variability interacts with storage limitations and demand growth. Although the tested climate change scenarios did not indicate a systematic worsening of water availability in the Aburrá Valley, the simulations highlighted important operational trade-offs, particularly between reduced reliance on pumping and increased security releases during extreme precipitation events. Simulation results further indicated a strong dependence on this supplemental inflow throughout the year, despite the reservoir operator statement that the pumping system operates during dry seasons. Additionally, a persistently high unmet demand ratio around 15% points to a fundamental limitation in the reservoir's ability to meet supply requirements due to its limited capacity.

Generally, the impacts of climate variability are more significant than land use change impacts [58], but land use management can be used to mitigate the excess of water resulting from the extreme events of precipitation enhancing the community resilience in the watersheds by implementing rainwater harvesting [59] and terrace farming [60], mostly in steep slope regions. These actions increase infiltration, reducing the peak of inflow to the reservoirs and subsequently the frequency and magnitude of security releases. In general, such increase in the catchment efficiency leads to an increase in the channel's baseflow resulting from the enhancement of slower soil transport processes.

The research was based on gridded climate datasets and reanalysis products, along with streamflow data derived from previous hydrological studies. Additional parameters were informed by news reports and publicly available information like bathymetry reports, compliance documents from the Superintendency of Public Services and other public reports to reservoir parametrization and operation formulation. While reasonable, the assumptions and hypothetical reservoir operation scenarios introduce uncertainties. These uncertainties can be reduced by the introduction of observed data. The presented approach is adaptable to other reservoir systems where operational rules, external inflows, and dynamic socio-environmental conditions play a significant role in water management. Future work should focus on incorporating observed operational data, constraining external water sources, and applying the method to interconnected reservoir networks to enhance regional-scale water security assessments.

5. Declaration of competing interest

We declare that we have no significant competing interests including financial or non-financial, professional, or personal interests interfering with the full and objective presentation of the work described in this manuscript.

6. Acknowledgements

The authors acknowledge the support provided by the Faculty of Engineering of the Universidad de Antioquia and the Graduate Program in Environmental Engineering.

7. Funding

The author(s) received no financial support for the research, authorship, and/or publication of this article.

8. Author contributions

N. Jastrombek Vieira conceived the idea, did the background research, collected the data, developed the workflow and code, and performed the assessment. *N. J. Aguirre Ramírez* and F. J. Vélez Macías supervised the research and provided critical feedback. *N. Jastrombek Vieira* led the manuscript writing, with contributions from all authors.

9. Data availability statement

The data supporting the findings of this study are publicly available from the sources cited in the manuscript. Additional processed data and model outputs are available from the corresponding author upon reasonable request.

10. Appendices

A. resv_dyn.py algorithm

The following routine calculates the reservoir dynamics for provided vectors of climatic data: observation time (time), daily inflow volume (inflow), daily precipitation over the reservoir (pcp_rate), daily evaporation over the reservoir (evap_rate), the corresponding population values (population) and the initial reservoir volume (vol_init). The relevant function is evolve_period and the remaining are auxiliary functions. In the following version the parameters for the La Fe reservoir are used, but the usage for the Riogrande II reservoir is analogous.

```
import pandas as pd

# LA_FE
vol_nom = 11.33e6                   # principal volume
vol_min = 0.1942 * vol_nom          # dead volume
vol_mid = 0.5137 * vol_nom          # technical minimum
vol_max = 13.53e6                   # emergency volume

city_demand_frac = 0.5
ref_population = 3849641 # population relate to ref_use_rate_day (2021)
ref_use_rate_day = 4.6 * 60 * 60 * 24 # m³/s -> m³/day

extra_outflow_start_year = 2024
extra_outflow_end_year = 2080
extra_outflow = 0.6 * 60 * 60 * 24 # Rionegro starts in 2024
extra_population = extra_outflow * ref_population / ref_use_rate_day

extra_inflow_start_year = 2011
extra_inflow_end_year = 2080
extra_inflow_slow = 3.0 * 60 * 60 * 24
extra_inflow_fast = 6.0 * 60 * 60 * 24

# demands take into account water distribution system: do not add more sinks that there are
person_demand_day = ref_use_rate_day /(ref_population * city_demand_frac)
eco_demand_day = 4.35 * 60 * 60 * 24
reg_erg_demand_day = 0 * 60 * 60 * 24 # already included in person demand
min_erg_demand_day = 0 * 60 * 60 * 24 # already included in person demand

outflow_nom_days = 2
outflow_max_days = 1

def calc_demand(vol, population):
    base_demand = eco_demand_day +
                  city_demand_frac * person_demand_day * population
    if vol >= vol_mid:
        return base_demand + reg_erg_demand_day
    if vol < vol_mid:
        return base_demand + min_erg_demand_day

def calc_outflow(vol):
    if vol > 0.95*vol_max:
        return (vol - vol_nom)/outflow_max_days
    elif vol > vol_nom:
        return (vol - vol_nom)/outflow_nom_days
    else:
```

```
        return 0

def calc_outflow_dumb(vol):
    if vol > 0.95*vol_max:
        return (vol - vol_nom)
    elif vol > vol_nom:
        return (vol - vol_nom)
    else:
        return 0

def calc_extra_inflow(date, vol):
    if vol < vol_mid and date.year > extra_inflow_start_year and
       date.year < extra_inflow_end_year:
        return extra_inflow_fast
    elif vol < vol_nom and date.year > extra_inflow_start_year and
         date.year < extra_inflow_end_year:
        return extra_inflow_slow
    else:
        return 0

def evolve_one_day(date, vol, inflow, pcp_rate, evap_rate, population):
    evap = evap_rate * vol
    pcp = pcp_rate * vol
    demand = calc_demand(vol, population)
    withdraw = 0
    unmet_demand = 0
    if (vol > vol_min):
        unmet_demand = 0
        withdraw = demand
    else:
        unmet_demand = demand
        withdraw = 0

    outflow = calc_outflow(vol)

    # add extra inflow
    extra_inflow = calc_extra_inflow(date, vol)
    inflow = inflow + extra_inflow

    # the volume for the next day
    vol = vol + inflow + pcp - outflow - evap - withdraw
    return {'vol': vol, 'demand': demand, 'outflow': outflow,
            'withdraw': withdraw, 'unmet_demand': unmet_demand,
            'extra_inflow': extra_inflow }


def evolve_period(time, vol_init, inflow, pcp_rate, evap_rate,
                  population):
    vol = []
    pcp = []
    evap = []
    demand = []
    outflow = []
    withdraw = []
    unmet_demand = []
```

```
extra_inflow = []
for i in range (len(time)):
    vol.append(vol_init)
    pcp.append(vol_init * pcp_rate[i])
    evap.append(vol_init * evap_rate[i])
    corr_population = population[i]
    if time[i].year >= extra_outflow_start_year and time[i].year <
       extra_outflow_end_year:
        corr_population += extra_population
    evo = evolve_one_day(time[i], vol_init, inflow[i], pcp_rate[i],
          evap_rate[i], corr_population)
    demand.append(evo['demand'])
    outflow.append(evo['outflow'])
    withdraw.append(evo['withdraw'])
    unmet_demand.append(evo['unmet_demand'])
    extra_inflow.append(evo['extra_inflow'])
    vol_init = evo['vol']

df = pd.DataFrame({
    'time': time,
    'Inflow_m3': inflow,
    'Outflow_m3': outflow,
    'StorageFlow_m3': vol,
    'Demand_m3': demand,
    'Withdrawal_m3': withdraw,
    'Unmet_demand_m3': unmet_demand,
    'pcp_m3': pcp,
    'evap_m3': evap,
    'extra_inflow_m3': extra_inflow
    })
return df
```

B. Population projection

Table 4 presents the urban population data from DANE national censuses and municipal projections for 2020–2035, which were used to fit the logistic curve model.

Table 4 Urban population of the municipalities in the Metropolitan Area of the Aburrá Valley reported in each national census and the DANE projections for the period 2020-2035. MED: Medellín, BAR: Barbosa, BEL:Bello, CAL: Caldas, COP: Copacabana, GIR: Girardota, ITA: Itagüí, EST: La Estrella, ENV+SAB: Envigado and Sabaneta.

Year	MED	BAR	BEL	CAL	COP	GIR	ITA	EST	ENV+SAB
1938	143,952	1,740	8,180	2,847	1,763	2,038	6,659	5,753	4,253
1951	328,294	2,763	28,398	5,846	2,673	2,481	11,027	2,864	13,392
1964	740,311	4,782	87,658	17,704	9,665	4,936	60,318	6,175	47,870
1973	1,122,099	7,830	103,039	28,635	21,231	11,022	90,828	14,533	76,523
1985	1,431,462	11,823	208,439	37,173	29,365	12,729	137,215	17,964	104,579
1993	1,551,160	13,379	257,711	45,251	39,621	17,131	175,626	33,626	130,766
2005	2,183,557	18,721	359,404	52,632	53,033	25,195	213,297	28,538	202,270
2018	2,320,248	21,469	456,897	61,442	62,102	27,896	234,939	57,451	271,842
2020	2,476,569	23,771	529,036	66,917	66,311	30,574	263,685	64,775	306,545
2021	2,506,656	24,868	536,766	68,174	67,553	31,615	267,720	65,928	311,398
2022	2,530,398	25,639	541,917	69,100	68,442	32,324	270,612	66,702	314,539
2023	2,553,621	26,343	546,902	69,957	69,303	32,970	273,385	67,454	317,539
2024	2,574,994	26,808	551,525	70,755	70,051	33,458	275,959	68,149	320,330
2025	2,593,542	27,216	555,509	71,410	70,691	33,900	278,179	68,734	322,772
2026	2,609,841	27,547	559,020	72,014	71,263	34,267	280,103	69,237	324,895
2027	2,624,783	27,825	562,182	72,518	71,790	34,590	281,856	69,695	326,755
2028	2,638,734	28,063	565,149	72,982	72,224	34,836	283,446	70,121	328,519
2029	2,651,875	28,234	567,955	73,385	72,623	35,069	284,915	70,483	330,135
2030	2,664,474	28,379	570,593	73,737	72,976	35,227	286,266	70,829	331,665
2031	2,676,581	28,499	573,087	74,055	73,321	35,378	287,538	71,159	333,084
2032	2,688,112	28,599	575,484	74,363	73,620	35,515	288,736	71,424	334,432
2033	2,698,987	28,699	577,760	74,647	73,896	35,623	289,866	71,715	335,705
2034	2,709,188	28,774	579,881	74,920	74,157	35,737	290,897	71,990	336,927
2035	2,718,758	28,865	581,834	75,152	74,407	35,835	291,878	72,228	338,018

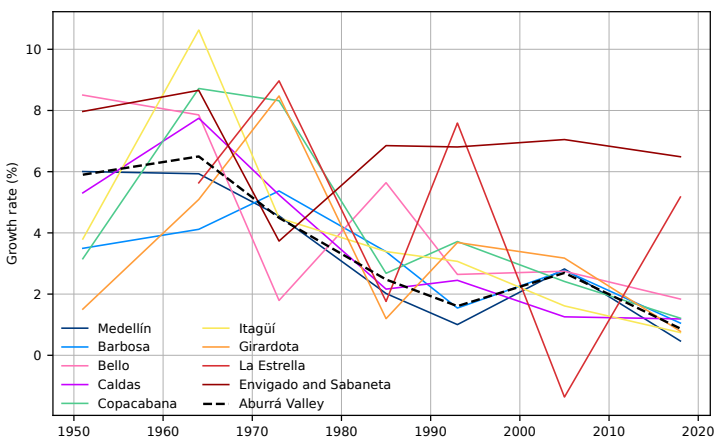

Figure 18 Relative annual population growth rate of the municipalities in the Metropolitan Area of the Aburrá Valley from 1951 to 2018. While most municipalities show a decreasing growth trend over time, Envigado and Sabaneta maintained a nearly constant growth rate from 1985 onward.

C. 3 Land use change model validation

The validation metrics, Figure of Merit (FoM), Producer's Accuracy, and User's Accuracy calculated from the error matrices through spatial overlay analysis are presented in Table 5. The land use change modeling results show varying levels of agreement between the simulated and observed maps for the two watersheds. For the Riogrande II watershed, the FoM was 28.31%, which is considered moderate and suggests that the model was able to capture a reasonable portion of actual land use changes. Producer's and User's accuracies were also similar, 43.22% and 43.83%, respectively, indicating balanced performance in terms of both the proportion of observed changes correctly simulated (Producer's Accuracy) and the proportion of predicted changes that were correct (User's Accuracy).

Table 5 Validation metrics of land use change model for Riogrande II watershed and La Fe watershed.

Metric	Riogrande II	La Fe
Figure of Merit (%)	28.31	11.96
Producer's Accuracy (%)	43.22	19.04
User's Accuracy (%)	43.83	22.67

In contrast, the model's performance for the La Fe watershed was lower, with a FoM of 11.96%, and Producer's and User's accuracies of 19.04% and 22.67%, respectively. These results suggest that the model had more difficulty capturing the detailed land use dynamics in La Fe. Although there are no universally accepted thresholds for these metrics, similar studies have reported FoM values ranging from 10% to 40% under realistic modeling scenarios (Pontius et al., 2008; Camacho Olmedo et al., 2015), supporting the interpretation of Riogrande's performance as good and La Fe's as acceptable. It is important to note that these metrics are calculated based on the spatial overlay of simulated and observed change maps. Therefore, they are strongly influenced by the resolution and precision of the spatial data. In this research, the land use maps have a spatial resolution of 30 meters, which poses a challenge for pixel-level agreement, especially when using probabilistic or stochastic models that estimate the likelihood of change rather than its exact location. Small spatial mismatches between predicted and observed changes can reduce the performance of these metrics, even when the model successfully captures broader patterns and quantities of change. To address this issue, a multiple window similarity analysis was performed. Figure 19 illustrates the similarity between the observed and simulated maps as a function of window size. The x-axis represents the number of pixels that define the side of a square analysis window: for example, a 3×3 window corresponds to an area of 90 meters per side, a 5×5 window to 150 meters, and so on. For stochastic land use models, a similarity above 50% is generally considered acceptable.

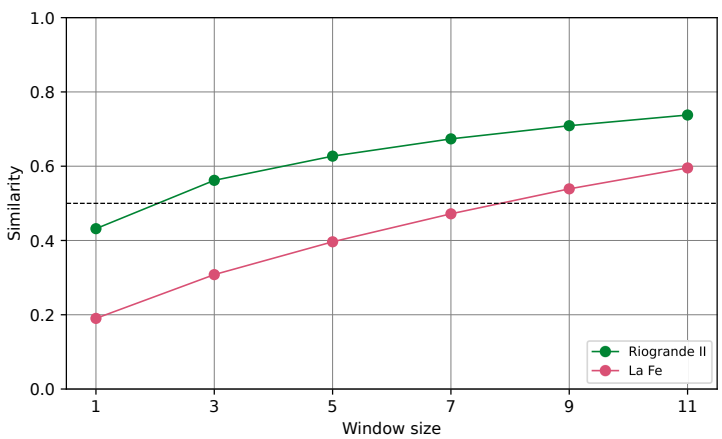

Figure 19 Multiple window similarity analysis for the Riogrande II and La Fe watershed.

As shown in the Figure 19, the Riogrande II model reaches the 50% similarity threshold with a window of just 2 pixels per side (i.e., 60 meters), indicating relatively strong spatial agreement even at finer resolutions. In contrast, the La Fe model reaches this threshold with a 240-meter window, suggesting lower spatial precision in replicating land use change patterns.

D. 4 SWAT+ Calibration and Validation

The calibrated parameters of monthly streamflow calibration using the Dynamically Dimensioned Search (DDS) algorithm after 500 iterations are presented in Table 6.

Table 6 Calibrated parameters for the SWAT+ model for both hydrographic basins.

Parameter	Change type	Riogrande II	La Fe
alpha	Replace	0.01	0.01
revap_min	Replace	0.00	0.01
flo_min	Replace	24.76	3.32
revap_co	Replace	0.04	0.03
sp_yld	Replace	-	0.28
awc	Relative	-30.00	10.00
k	Relative	21.05	20.00
cn2	Relative	30.00	20.00
ovn	Relative	-23.08	-20.00
cn3_swf	Replace	1.00	0.97
esco	Replace	0.09	0.76
epco	Replace	0.45	-
perco	Replace	0.73	0.37
petco	Replace	-	1.04
lat_len	Relative	-40.00	4.67
surlag	Replace	3.54	1.55

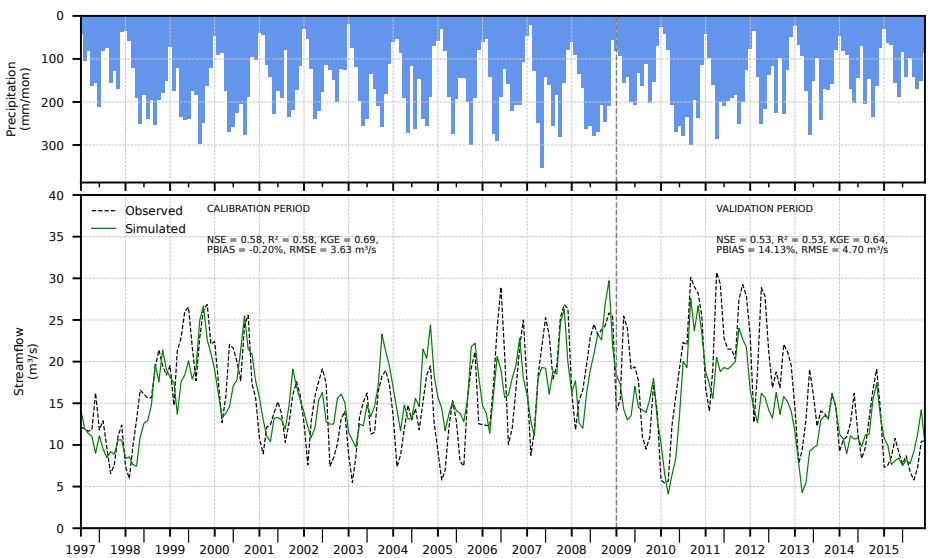

Figure 20 Calibration (1997–2008) and validation periods (2009–2015) of SWAT+ for monthly streamflow of Puente Belmira gauge station, Riogrande II reservoir watershed.

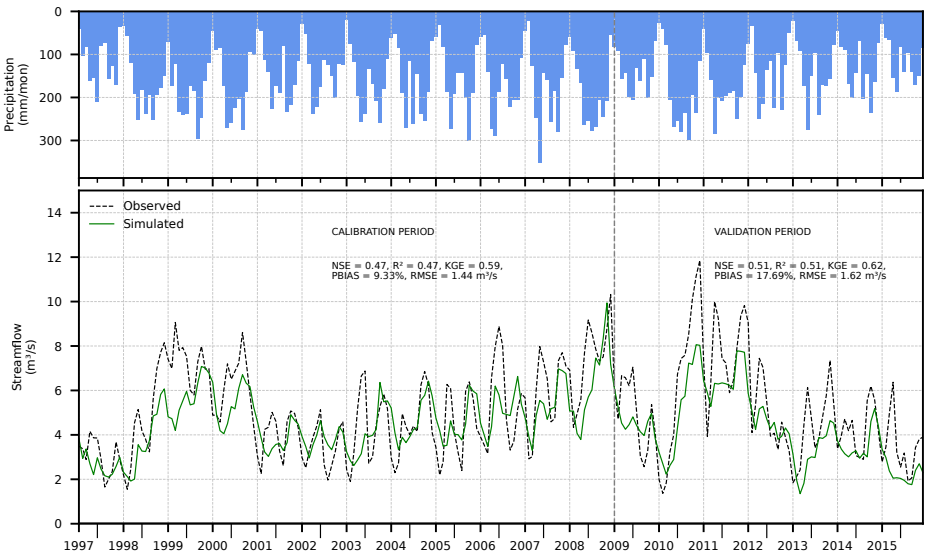

Figure 21 Calibration (1997–2008) and validation (2009–2015) of SWAT+ for monthly streamflow of Rio Chico gauge station, Riogrande II reservoir watershed.

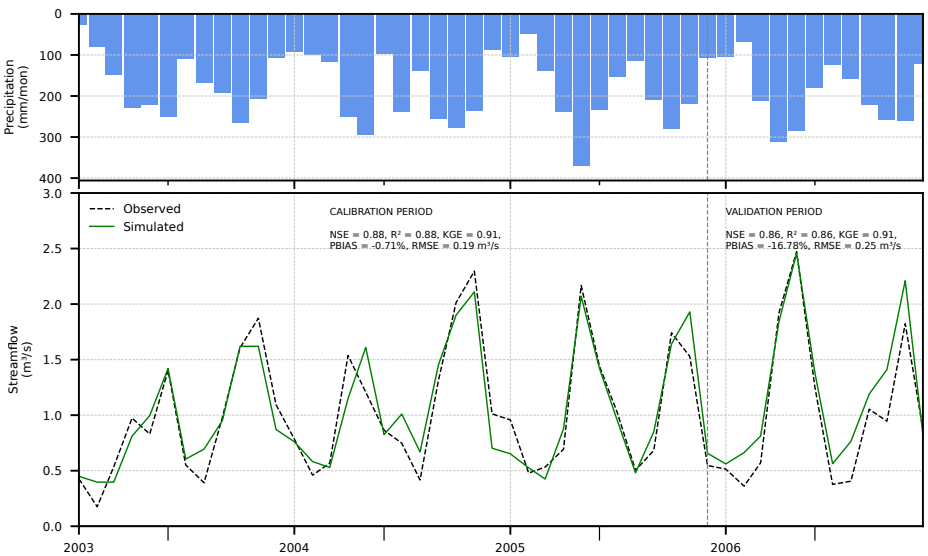

Figure 22 Calibration (2003–2005) and validation (2006) of SWAT+ for monthly streamflow of Quebrada Las Palmas gauge station, La Fe reservoir watershed.

References

[1] H. T. Aboelnga, L. Ribbe, F.-B. Frechen, and J. Saghir, "Urban Water Security: Definition and Assessment Framework," *Resources*, vol. 8, no. 4, p. 178, 2019, number: 4 Publisher: Multidisciplinary Digital Publishing Institute. [Online]. Available: https://www.mdpi.com/2079-9276/8/4/178

[2] EPM, "Presentación - Atención a medios - Modernización planta de potabilización Manantiales," 2024. [Online]. Available: https://www.epm.com.co/content/dam/epm/institucional/sala-de-prensa-epm/noticias-y-novedades/noticias-y-novedades/interrupcion-acueducto-norte-valle-aburra-epm/presentacion-manantiales-05-11-2024.pdf

[3] B. Shrestha, T. A. Cochrane, B. S. Caruso, M. E. Arias, and T. Piman, "Uncertainty in flow and sediment projections due to future climate scenarios for the 3S Rivers in the Mekong Basin," *Journal of Hydrology*, vol. 540, pp. 1088–1104, Sep. 2016. [Online]. Available: https://www.sciencedirect.com/science/article/pii/S0022169416304498

[4] F. Farinosi, M. E. Arias, E. Lee, M. Longo, F. F. Pereira, A. Livino, P. R. Moorcroft, and J. Briscoe, "Future Climate and Land Use Change Impacts on River Flows in the Tapajós Basin in the Brazilian Amazon," *Earth's Future*, vol. 7, no. 8, pp. 993–1017, 2019. [Online]. Available: https://onlinelibrary.wiley.com/doi/abs/10.1029/2019EF001198

[5] J. D. Pabón-Caicedo, P. A. Arias, A. F. Carril, J. C. Espinoza, L. F. Borrel, K. Goubanova, W. Lavado-Casimiro, M. Masiokas, S. Solman, and R. Villalba, "Observed and Projected Hydroclimate Changes in the Andes," *Frontiers in Earth Science*, vol. 8, Mar. 2020, publisher: Frontiers. [Online]. Available: https://www.frontiersin.orghttps://www.frontiersin.org/journals/earth-science/articles/10.3389/feart.2020.00061/full

[6] M. Flörke, E. Kynast, I. Bärlund, S. Eisner, F. Wimmer, and J. Alcamo, "Domestic and industrial water uses of the past 60 years as a mirror of socio-economic development: A global simulation study," *Global Environmental Change*, vol. 23, no. 1, pp. 144–156, Feb. 2013. [Online]. Available: https://www.sciencedirect.com/science/article/pii/S0959378012001318

[7] C. J. Vörösmarty, P. Green, J. Salisbury, and R. B. Lammers, "Global Water Resources: Vulnerability from Climate Change and Population Growth," *Science*, vol. 289, no. 5477, pp. 284–288, Jul. 2000, publisher: American Association for the Advancement of Science. [Online]. Available: https://www.science.org/doi/10.1126/science.289.5477.284

[8] Arnold, D. N. Moriasi, P. W. Gassman, K. C. Abbaspour, M. J. White, R. Srinivasan, C. Santhi, R. D. Harmel, A. Van Griensven, M. W. Van Liew, N. Kannan, and M. K. Jha, "SWAT: Model Use, Calibration, and Validation," *Transactions of the ASABE*, vol. 55, no. 4, pp. 1491–1508, 2012. [Online]. Available: http://elibrary.asabe.org/abstract.asp??JID=3&AID=42256&CID=t2012&v=55&i=4&T=1

[9] P. W. Gassman, A. M. Sadeghi, and R. Srinivasan, "Applications of the SWAT Model Special Section: Overview and Insights," *Journal of Environmental Quality*, vol. 43, no. 1, pp. 1–8, 2014. [Online]. Available: https://onlinelibrary.wiley.com/doi/abs/10.2134/jeq2013.11.0466

[10] A. Nguyen, C. , Thomas A., , and M. Pahlow, "Optimising water allocation and land management to mitigate the effects of land use and climate change on reservoir performance," *Hydrological Sciences Journal*, vol. 67, no. 14, pp. 2129–2146, Oct. 2022, publisher: Taylor & Francis _eprint: https://doi.org/10.1080/02626667.2022.2132162. [Online]. Available: https://doi.org/10.1080/02626667.2022.2132162

[11] C. M. Almeida, J. M. Gleriani, E. F. Castejon, and B. S. Soares-Filho, "Using neural networks and cellular automata for modelling intra-urban land-use dynamics," *International Journal of Geographical Information Science*, vol. 22, no. 9, pp. 943–963, Sep. 2008, number: 9 Publisher: Taylor & Francis _eprint: https://doi.org/10.1080/13658810701731168. [Online]. Available: https://doi.org/10.1080/13658810701731168

[12] B. Soares-Filho, H. Rodrigues, and M. Follador, "A hybrid analytical-heuristic method for calibrating land-use change models," *Environmental Modelling & Software*, vol. 43, pp. 80–87, May 2013. [Online]. Available: https://www.sciencedirect.com/science/article/pii/S1364815213000236

[13] H. Rodrigues and B. Soares-Filho, "A Short Presentation of Dinamica EGO," in *Geomatic Approaches for Modeling Land Change Scenarios*, M. T. Camacho Olmedo, M. Paegelow, J.-F. Mas, and F. Escobar, Eds. Cham: Springer International Publishing, 2018, pp. 493–498. [Online]. Available: https://doi.org/10.1007/978-3-319-60801-3_35

[14] M. P. S. Giraldo, "Water Distribution and Drainage Systems of Aburrá Valley, Colombia – Empresas Públicas de Medellín E.S.P." *Procedia Engineering*, vol. 186, pp. 4–11, Jan. 2017. [Online]. Available: https://www.sciencedirect.com/science/article/pii/S1877705817313383

[15] J. Ossa, Ana Karina Campillo, Cristian Omar, and Teresita Betancur, "Representación espacial de zonas de recarga del agua subterránea a partir de mapas isotópicos de precipitación. Caso de estudio: Valle de Aburrá, Colombia," *BOLETÍN GEOLÓGICO Y MINERO*, vol. 132, no. 1-2, pp. 65–75, Jun. 2021, number: 1-2. [Online]. Available: http://www.igme.es/boletin/2021/132_1-2/BGM_132-1-2_Art-7.pdf

[16] E. Aristizábal, E. F. Garcia, R. J. Marin, F. Gómez, J. Guzmán-Martínez, E. Aristizábal, E. F. Garcia, R. J. Marin, F. Gómez, and J. Guzmán-Martínez, "Rainfall-intensity effect on landslide hazard assessment due to climate change in north-western Colombian Andes," *Revista Facultad de Ingeniería Universidad de Antioquia*, no. 103, pp. 51–66, Jun. 2022, publisher: Universidad de Antioquia. [Online]. Available: http://www.scielo.org.co/scielo.php?script=sci_abstract&pid=S0120-62302022000200051&lng=en&nrm=iso&tlng=en

[17] C. N. d. O. CNO, "Acuerdo 1924 Por el cual se aprueba la actualización de unos parámetros técnicos de los volúmenes del embalse Ríogrande II | Consejo nacional de operación del sector eléctrico CNO," 2025. [Online]. Available: https://www.cno.org.co/content/acuerdo-1924-por-el-cual-se-aprueba-la-actualizacion-de-unos-parametros-

[18] M. T. Flórez Molina, L. N. Parra Sánchez, S. V. Bolaños Benitez, L. J. Gallo Sánchez, A. M. Poveda Sáenz, and D. M. Agudelo Echavarría, "Tasas de sedimentación y características de sedimentos de fondo en tres embalses de Antioquia, Colombia," *Ingeniería del agua*, vol. 22, no. 4, pp. 177–194, Oct. 2018, number: 4. [Online]. Available: https://doi.org/10.4995/ia.2018.8001

[19] M. Colombia, "Colección 1 de la Serie anual de Mapas de Cobertura y Uso del Suelo de Colombia," 2024. [Online]. Available: https://colombia.mapbiomas.org/descargas/

[20] A. López-Ballesteros, A. Nielsen, G. Castellanos-Osorio, D. Trolle, and J. Senent-Aparicio, "DSOLMap, a novel high-resolution global digital soil property map for the SWAT + model: Development and hydrological evaluation," *CATENA*, vol. 231, p. 107339, Oct. 2023. [Online]. Available: https://www.sciencedirect.com/science/article/pii/S0341816223004307

[21] EPM, "Plantas de potabilización," Oct. 2023. [Online].

Available: https://www.epm.com.co/institucional/sobre-epm/nuestras-plantas/plantas-de-agua.html
[22] S. S. P. Domiciliarios, "Evaluación de prestadores," 2021. [Online]. Available: https://www.superservicios.gov.co/Empresas-vigiladas/Acueducto-alcantarillado-y-aseo/Acueducto-y-alcantarillado/Evaluacion-de-prestadores
[23] F. Amaringo, Y. Puerta, and F. Molina, "Probabilistic Risk Assessment of Polycyclic Aromatic Hydrocarbons in a Colombian Reservoir," *Bulletin of Environmental Contamination and Toxicology*, vol. 109, no. 3, pp. 518–525, Sep. 2022, number: 3. [Online]. Available: https://doi.org/10.1007/s00128-022-03567-7
[24] D. G. Ramírez, J. F. Narváez Valderrama, C. A. Palacio Tobón, J. J. García, J. D. Echeverri, J. Sobotka, and B. Vrana, "Occurrence, sources, and spatial variation of POPs in a mountainous tropical drinking water supply basin by passive sampling," *Environmental Pollution*, vol. 318, p. 120904, Feb. 2023. [Online]. Available: https://www.sciencedirect.com/science/article/pii/S0269749122021194
[25] DANE, "CENSO GENERAL DE POBLACIÓN 1938 : DEPARTAMENTO DE ANTIOQUIA," 1938. [Online]. Available: https://biblioteca.dane.gov.co/biblioteca/books/3/
[26] ——, "CENSO DE POBLACIÓN DE 1951 : DEPARTAMENTO DE ANTIOQUIA," 1951. [Online]. Available: https://biblioteca.dane.gov.co/biblioteca/books/20/
[27] ——, "XIII CENSO NACIONAL DE POBLACIÓN 1964 : ANTIOQUIA," 1964. [Online]. Available: https://biblioteca.dane.gov.co/biblioteca/books/176/
[28] ——, "XIV CENSO NACIONAL DE POBLACIÓN Y III DE VIVIENDA 1973 : DEPARTAMENTO DE ANTIOQUIA," 1973. [Online]. Available: https://biblioteca.dane.gov.co/biblioteca/books/84/
[29] ——, "XV CENSO NACIONAL DE POBLACIÓN Y IV DE VIVIENDA 1985. COLOMBIA - CENSO 1985," 1985. [Online]. Available: https://biblioteca.dane.gov.co/biblioteca/books/106/
[30] ——, "XVI CENSO NACIONAL DE POBLACIÓN Y V DE VIVIENDA 1993 : ANTIOQUIA," 1993. [Online]. Available: https://biblioteca.dane.gov.co/biblioteca/books/110/
[31] ——, "Censo general 2005," 2005. [Online]. Available: https://www.dane.gov.co/files/censos/libroCenso2005nacional.pdf
[32] ——, "Censo Nacional de Población y Vivienda – CNPV 2018," 2018, anexo Población ajustada por cobertura. [Online]. Available: https://www.dane.gov.co/index.php/estadisticas-por-tema/demografia-y-poblacion/censo-nacional-de-poblacion-y-vivienda-2018/informacion-tecnica
[33] ——, "Proyecciones y retroproyecciones de población municipal para el periodo 1985-2017 y 2018-2042 con base en el CNPV 2018," 2023. [Online]. Available: https://www.dane.gov.co/index.php/estadisticas-por-tema/demografia-y-poblacion/proyecciones-de-poblacion
[34] L.-F. et al., "Modeling Environmental Dynamics with Dinamica EGO," 2020. [Online]. Available: https://dinamicaego.com/dokuwiki/doku.php?id=guidebook_start
[35] M. Colombia, "ATBD (Documento Base Teórico de Algoritmos)," 2025. [Online]. Available: https://colombia.mapbiomas.org/atbd/
[36] P. A. Arias, G. Ortega, L. D. Villegas, and J. A. Martínez, "Colombian climatology in CMIP5/CMIP6 models: Persistent biases and improvements," *Revista Facultad de Ingeniería Universidad de Antioquia*, no. 100, pp. 75–96, May 2021, number: 100. [Online]. Available: https://revistas.udea.edu.co/index.php/ingenieria/article/view/344493
[37] G. Ortega, P. A. Arias, J. C. Villegas, P. A. Marquet, and P. Nobre, "Present-day and future climate over central and South America according to CMIP5/CMIP6 models," *International Journal of Climatology*, vol. 41, no. 15, pp. 6713–6735, 2021. [Online]. Available: https://onlinelibrary.wiley.com/doi/abs/10.1002/joc.7221
[38] A. Adcroft, W. Anderson, V. Balaji, C. Blanton, M. Bushuk, C. O. Dufour, J. P. Dunne, S. M. Griffies, R. Hallberg, M. J. Harrison, I. M. Held, M. F. Jansen, J. G. John, J. P. Krasting, A. R. Langenhorst, S. Legg, Z. Liang, C. McHugh, A. Radhakrishnan, B. G. Reichl, T. Rosati, B. L. Samuels, A. Shao, R. Stouffer, M. Winton, A. T. Wittenberg, B. Xiang, N. Zadeh, and R. Zhang, "The GFDL Global Ocean and Sea Ice Model OM4.0: Model Description and Simulation Features," *Journal of Advances in Modeling Earth Systems*, vol. 11, no. 10, pp. 3167–3211, 2019. [Online]. Available: https://agupubs.onlinelibrary.wiley.com/doi/10.1029/2019MS001726
[39] B. C. O'Neill, E. Kriegler, K. L. Ebi, E. Kemp-Benedict, K. Riahi, D. S. Rothman, B. J. van Ruijven, D. P. van Vuuren, J. Birkmann, K. Kok, M. Levy, and W. Solecki, "The roads ahead: Narratives for shared socioeconomic pathways describing world futures in the 21st century," *Global Environmental Change*, vol. 42, pp. 169–180, Jan. 2017, publisher: Elsevier. [Online]. Available: https://pure.iiasa.ac.at/id/eprint/11293/,https://iiasa.dev.local/
[40] "Summary for Policymakers," in *Climate Change 2021 – The Physical Science Basis: Working Group I Contribution to the Sixth Assessment Report of the Intergovernmental Panel on Climate Change*, IPCC - Intergovernmental Panel on Climate Change (IPCC), Ed. Cambridge: Cambridge University Press, 2023, pp. 3–32. [Online]. Available: https://www.cambridge.org/core/books/climate-change-2021-the-physical-science-basis/summary-for-policymakers/8E7A4E3AE6C364220F3B76A189CC4D4C
[41] F. Lehner, I. Nadeem, and H. Formayer, "Evaluating quantile-based bias adjustment methods for climate change scenarios," *Hydrology and Earth System Sciences Discussions*, pp. 1–26, Nov. 2021, publisher: Copernicus GmbH. [Online]. Available: https://hess.copernicus.org/preprints/hess-2021-498/
[42] A. J. Cannon, S. R. Sobie, and T. Q. Murdock, "Bias Correction of GCM Precipitation by Quantile Mapping: How Well Do Methods Preserve Changes in Quantiles and Extremes?" Sep. 2015, section: Journal of Climate. [Online]. Available: https://journals.ametsoc.org/view/journals/clim/28/17/jcli-d-14-00754.1.xml
[43] P. Bourgault, D. Huard, T. J. Smith, T. Logan, A. Aoun, J. Lavoie, . Dupuis, G. Rondeau-Genesse, R. Alegre, C. Barnes, A. B. Laperrière, S. Biner, D. Caron, C. Ehbrecht, J. Fyke, T. Keel, M.-P. Labonté, L. Lierhammer, J.-F. Low, J. Quinn, P. Roy, D. Squire, A. Stephens, M. Tanguy, and C. Whelan, "xclim: xarray-based climate data analytics," *Journal of Open Source Software*, vol. 8, no. 85, p. 5415, May 2023. [Online]. Available: https://joss.theoj.org/papers/10.21105/joss.05415
[44] A. DAAC, "ALOS PALSAR High Resolution Radiometric Terrain Corrected Product [Dataset]," Dec. 2024. [Online]. Available: https://www.earthdata.nasa.gov/data/catalog/asf-alos-psr-rtc-high-1
[45] C. Funk, P. Peterson, M. Landsfeld, D. Pedreros, J. Verdin, S. Shukla, G. Husak, J. Rowland, L. Harrison, A. Hoell, and J. Michaelsen, "The climate hazards infrared precipitation with stations—a new environmental record for monitoring extremes," *Scientific Data*, vol. 2, no. 1, p. 150066, Dec. 2015, publisher: Nature Publishing Group. [Online]. Available: https://www.nature.com/articles/sdata201566
[46] H. Hersbach, B. Bell, P. Berrisford, G. Biavati, A. Horányi,

J. Muñoz Sabater, J. Nicolas, C. Peubey, R. Radu, I. Rozum, D. Schepers, A. Simmons, C. Soci, D. Dee, and J.-N. Thépaut, "ERA5 hourly data on single levels from 1940 to present," 2023. [Online]. Available: 10.24381/cds.adbb2d47

[47] S. Valencia, D. E. Marín, D. Gómez, N. Hoyos, J. F. Salazar, and J. C. Villegas, "Spatio-temporal assessment of Gridded precipitation products across topographic and climatic gradients in Colombia," *Atmospheric Research*, vol. 285, p. 106643, Apr. 2023. [Online]. Available: https://www.sciencedirect.com/science/article/pii/S0169809523000406

[48] C. H. B. Priestley and R. J. Taylor, "On the Assessment of Surface Heat Flux and Evaporation Using Large-Scale Parameters," Feb. 1972, section: Monthly Weather Review. [Online]. Available: https://journals.ametsoc.org/view/journals/mwre/100/2/1520-0493_1972_100_0081_otaosh_2_3_co_2.xml

[49] Chow, "Applied Hydrology," 1988.

[50] B. A. Tolson and C. A. Shoemaker, "Dynamically dimensioned search algorithm for computationally efficient watershed model calibration," *Water Resources Research*, vol. 43, no. 1, 2007. [Online]. Available: https://onlinelibrary.wiley.com/doi/abs/10.1029/2005WR004723

[51] N. Uribe, R. Srinivasan, G. Corzo, D. Arango, and D. Solomatine, "Spatio-temporal critical source area patterns of runoff pollution from agricultural practices in the Colombian Andes," *Ecological Engineering*, vol. 149, p. 105810, Apr. 2020. [Online]. Available: https://www.sciencedirect.com/science/article/pii/S0925857420300987

[52] S. Valencia, J. C. Villegas, N. Hoyos, M. Duque-Villegas, and J. F. Salazar, "Streamflow response to land use/land cover change in the tropical Andes using multiple SWAT model variants," *Journal of Hydrology: Regional Studies*, vol. 54, p. 101888, Aug. 2024. [Online]. Available: https://linkinghub.elsevier.com/retrieve/pii/S2214581824002374

[53] Área Metropolitana del valle de Aburrá, Universidad Nacional de Colombia sede Medelín, CORANTIOQUIA, and CORNARE, "Plan de Ordenación y Manejo de Cuenca Hidrográfica - Rio Aburrá," 2008. [Online]. Available: https://www.metropol.gov.co/ambiental/recurso-hidrico/pomca/2007/pomca-c2-subsistema-abiotico-recursoagua.pdf

[54] CORANTIOQUIA, "ACTUALIZACIÓN Y AJUSTE PLAN DE ORDENACIÓN Y MANEJO DE LA CUENCA DE LOS RÍOS GRANDE Y CHICO," 2015.

[55] Cornare, "SEGUIMIENTO ANUAL 2022, AL PLAN DE ORDENAMIENTO DEL RECURSO HÍDRICO-PORH Y LOS OBJETIVOS DE CALIDAD ESTABLECIDOS MEDIANTE LA RESOLUCIÓN N°112-5304 DEL 26 DE OCTUBRE DE 2016," 2023.

[56] EPM, "Análisis de la información batimétrica del embalse Riogrande II," 2015.

[57] ——, "Resultados Batimetría embalses La Fe y Quebradona," 2019.

[58] G. S. Dwarakish and B. P. Ganasri, "(PDF) Impact of land use change on hydrological systems: A review of current modeling approaches," *ResearchGate*, 2015. [Online]. Available: https://www.researchgate.net/publication/287374409_Impact_of_land_use_change_on_hydrological_systems_A_review_of_current_modeling_approaches

[59] Eta, E. G. F, I. F. O, A. C. F, and N. G. C, "Climate Change And Rural Farmers' Water Shortage Coping Mechanisms In Idemili North Agricultural Block, Anambra State, Nigeria," *Global Journal of Agricultural Sciences*, vol. 24, no. 1, pp. 105–110, May 2025, number: 1. [Online]. Available: https://www.ajol.info/index.php/gjass/article/view/296328

[60] T. Sarkar and S. Sengupta, Eds., *Cultivating Progress: New Frontiers in Agricultural Science and Technology*, 1st ed. AkiNik Publications, Jan. 2025. [Online]. Available: https://www.akinik.com/products/3189/cultivating-progress-new-frontiers-in-agricultural-science-and-technology

[61] W. Q. Wang and H. Shao, "High altitude platform multichannel SAR for wide-area and staring imaging," *Aerosp. and Electron. Syst.*, vol. 29, no. 25, pp. 12–17, Mar. 2014.